PHOTONICS Research

Broadband high-efficiency plasmonic metalens with negative dispersion characteristic

Yong-Qiang Liu,* Yong Zhu, Hongcheng Yin, Jinhai Sun, Yan Wang, and Yongxing Che

National Key Laboratory of Scattering and Radiation, Beijing 100854, China
**Corresponding author: liuyq1990@126.com*

Received 22 November 2023; revised 5 February 2024; accepted 20 February 2024; posted 21 February 2024 (Doc. ID 513990); published 1 April 2024

Controlling the dispersion characteristic of metasurfaces (or metalenses) along a broad bandwidth is of great importance to develop high-performance broadband metadevices. Different from traditional lenses that rely on the material refractive index along the light trajectory, metasurfaces or metalenses provide a new regime of dispersion control via a sub-wavelength metastructure, which is known as negative chromatic dispersion. However, broadband metalenses design with high-performance focusing especially with a reduced device dimension is a significant challenge in society. Here, we design, fabricate, and demonstrate a broadband high-performance diffractive-type plasmonic metalens based on a circular split-ring resonator metasurface with a relative working bandwidth of 28.6%. The metalens thickness is only $0.09\lambda_0$ (λ_0 is at the central wavelength), which is much thinner than previous broadband all-dielectric metalenses. The full-wave simulation results show that both high transmissive efficiency above 80% (the maximum is even above 90%) and high average focusing efficiency above 45% (the maximum is 56%) are achieved within the entire working bandwidth of 9–12 GHz. Moreover, an average high numerical aperture of 0.7 (NA = 0.7) of high-efficiency microwave metalens is obtained in the simulations. The broadband high-performance metalens is also fabricated and experimental measurements verify its much higher average focusing efficiency of 55% (the maximum is above 65% within the broad bandwidth) and a moderate high NA of 0.6. The proposed plasmonic metalens can facilitate the development of wavelength-dependent broadband diffractive devices and is also meaningful to further studies on arbitrary dispersion control in diffractive optics based on plasmonic metasurfaces. © 2024 Chinese Laser Press

https://doi.org/10.1364/PRJ.513990

1. INTRODUCTION

Microwave and optical devices such as prisms, reflectors, gratings, or lenses are indispensable in modern science and technology, and their high-quality developments represent significant technical achievements in the history of humankind. These traditional elements mostly rely on the phase change along the light trajectory inside three-dimensional structures, which leads to the whole devices usually being very bulky and heavy, which limits their further applications for some miniaturized and integrated systems.

Over the last decade, there has been much interest focusing on two-dimensional (2-D) ultra-thin periodical metallic or dielectric structures, namely metasurfaces or metastructures to design various functional devices and systems. In addition, the working principles can be controlled by the generalized laws of reflection and/or refraction [1]. Among these, metasurface lenses (or metalenses) are an important metadevice and have become an active research field in recent years owing to their superior performances and much lower profile design compared to traditional designs [2–8].

The dispersion property of most materials and devices is positive, which relies on the traditional refractive laws. This is intrinsically caused by their increased refractive index along with increased frequency range. For example, prisms deflect more blue light than red light with larger refractive angle. As a result, traditional microwave or optical refractive lenses focus incident waves of larger operation frequency on the focal plane with smaller focal length. This phenomenon is schematically illustrated in Fig. 1(a). For incident waves with larger operation frequency of f_1, its larger refractive angle leads to smaller focal length of F_1 because of the above-mentioned normal material dispersion. Another important type of negative dispersion control is typical diffractive devices such as conventional Fresnel lenses or blazed grating [9–11] which have long existed in the optical and/or microwave society. Diffractive-type devices and systems demonstrate a larger focal length of F_1 with a larger operation frequency of incident wave f_1 which is originally caused by an interference effect, as shown in Fig. 1(b).

Recent studies and advancements demonstrate that metasurfaces or metalenses dispersion is more like that of

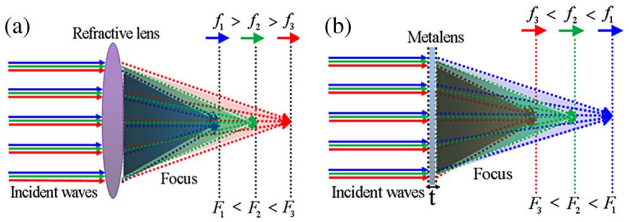

Fig. 1. (a) Scheme of refractive lens dispersion property with broadband incident wave frequency from f_1 to f_3. The relative relation of positive dispersion is explained by inverse focal length of $F_1 < F_2 < F_3$ for $f_1 > f_2 > f_3$. (b) Negative dispersion relation illustration in the proposed broadband metalens for incident wave frequency of $f_1 > f_2 > f_3$; its focal length is positively proportional of $F_1 > F_2 > F_3$.

diffractive-type since their constitute elements are various sub-wavelength 2-D dielectric or metallic patterned geometric structures [4,5,12–16]. Controlling the fundamental chromatic dispersion in metasurfaces or metalenses is of great importance and also has attracted great interest in recent years [12–30]. It should be noted that these progress and achievements are mainly obtained for the all-dielectric metasurfaces or metalenses in the high-frequency band such as in the visible or infrared regimes. On the other hand, metalens designs by using plasmonic or metallic metasurfaces in a low spectrum such as terahertz (THz) or microwave are also presented but most designs suffer from low efficiency or low NA especially for a continuous broadband range [31–42]. In order to improve their transmission performances and extend their phase control range, multi-layer metallic metasurfaces of at least three or more are commonly used as a meta-atom which makes the whole device bulky and need multiple fabrication processes and strict alignments [43–56]. Some broadband metalens designs even adopt and combine different metasurface shapes which also pose a great challenge for practical applications [35–37]. Very recently, an ultra-thin double-layer broadband high focusing efficiency of above 40% for a plasmonic metalens from 8.0 to 10.5 GHz was demonstrated and reported in the microwave band but the dispersion characteristic is still traditional refractive-type [38]. To design plasmonic metalenses with broader bandwidth and higher efficiency by using a reduced device thickness is urgent especially for a diffractive-type dispersion property, which can enrich the studies on broadband high-performance plasmonic metalenses in the community [31–38].

In this paper, an ultra-thin broadband plasmonic metalens from 9 to 12 GHz based on a bi-layer phase gradient circular split-ring metasurface is designed, fabricated, and characterized both numerically and experimentally. Both high transmissive efficiency and high focusing efficiency in the entire operation bandwidth are realized in the simulations. In addition, a moderate high NA is also achieved. Experimental measurement results also verify its high focusing efficiency for the designed broadband metalens. These excellent focusing performances can outperform previous broadband plasmonic metalenses largely in low spectra [31–38]. Furthermore, both numerical and experimental results of wavelength-dependent focusing demonstrate its diffractive-type dispersion property which is also ready for numerous applications such as wideband and high-gain transmitarray antennas [43–56].

2. PRINCIPLE OF DISPERSION CONTROL FOR PLASMONIC METALENS

Chromatic dispersion control of sub-wavelength metalenses in the high-frequency band is usually based on the multiple parameters optimizations of the all-dielectric meta-atom on the substrate [19–22]. In addition, some broadband achromatic metalenses are also obtained by combining different types of meta-atoms by controlling the phase and phase slope of the meta-atom simultaneously. Although the chromatic dispersion can degrade imaging performances for some applications, its intrinsic dispersion property, especially diffractive-type along broadband frequency in low spectra, is of great importance for some novel applications such as wideband microwave transmitarray antennas [43–56], nanoparticle trapping [57,58], edge detection [59,60], and broadband retroreflectors [61–63]. Additionally, understanding its original dispersion of single plasmonic metalens simultaneously with high-performance focusing properties can pave the way for further studies on broadband achromatic metalenses [36,37]. The dispersion issues for plasmonic metalenses are not well addressed and talked about so far because of their complicated multi-layer metal–dielectric configurations [31–38]. Here, we first give the general dispersion control condition for broadband plasmonic metalens design and then demonstrate an ultra-thin broadband diffractive-type microwave metalens both numerically and experimentally. In order to realize broadband and highly-efficient focusing for normally incident waves, the frequency f and focal length F dependent quadratic phase profile should be satisfied as follows [17–38]:

$$\varphi(f,F) = \frac{2\pi f}{c}\left(\sqrt{r^2+F^2}\right). \tag{1}$$

For most cases, this radial position r-dependent phase profile varies for a broadband frequency range; thus, its focal length F is also different with different operation frequency f, i.e., the well-known chromatic dispersion. c is light speed in free space. This chromatic dispersion commonly exists in low spectra with plasmonic metasurfaces [31–38]. To give a close look at its dispersion characteristic along a broadband frequency range, we should calculate its phase-shift differential equation which includes two variables, i.e., f and F. Hence, the following expression can de deduced and obtained:

$$\mathrm{d}\varphi = \frac{2\pi}{c}\left(\sqrt{r^2+F^2}\right) + \frac{2\pi f}{c}\frac{F}{\sqrt{r^2+F^2}}. \tag{2}$$

It can be noted that the key to control its dispersion property is the simultaneous control of the phase φ and its phase-shift slope $\mathrm{d}\varphi$ of plasmonic meta-atom carefully [17–21]. Some broadband plasmonic metalenses in the THz or microwave spectrum are demonstrated by using triple-layer metasurfaces [31–35], but the working efficiency and NA are relatively low. More importantly, the dispersion characteristic of these broadband plasmonic metalenses is inconclusive [31–35,38], which hinders its further studies on arbitrary dispersion control based on plasmonic metasurfaces. There is only one

double-layer refractive-type high-efficiency broadband plasmonic metalens in the microwave regime [38]. There are two basic conditions for a broadband plasmonic metalens realization according to the above expressions. The first is that the phase change range of the proposed meta-atom along a broadband frequency range should be linear as much as possible. Second, the phase slope in Eq. (2) should change faster than the designed focal length for the considered broadband frequency range for the refractive-type dispersion while the inverse condition for diffractive-type dispersion [31–35,38]. An achromatic doublet lens with opposite dispersion such as the combination of refractive-type and diffractive-type can pave the way for further broadband microwave studies but reducing its whole device thickness is still very challenging according to some recent studies [35–37].

3. UNIT CELL DESIGN AND BROADBAND PLASMONIC METALENS PERFORMANCES

A. Unit Cell Design and Full-Wave Simulations

Different from previous broadband metallic metalenses based on multi-layer patch metasurfaces patterned on the dielectric media [31–35], we here propose an ultra-thin double-layer symmetric complementary circular split-ring resonator (SRR) metasurface to design frequency-dependent broadband metalenses, which only need a single-step fabrication process. In addition, the complementary SRR metastructure can realize higher transmission magnitude compared to previous square or circular patched ones [32–35], which can be very promising to design high-performance plasmonic metalenses in low spectra. The single-layer simple configuration can largely reduce the design complexity and ease the device burden and fabrication cost. Figure 2(a) plots the perspective views of the identical double-layer SRR metasurface which is sandwiched by the filled dielectric medium (dielectric permittivity $\varepsilon = 2.2$) in between with a device thickness of $t = 2.6$ mm. The whole device thickness is only $0.09\lambda_0$ (λ_0 is at the central wavelength), which is much thinner than previous broadband all-dielectric metalenses [12–30] and plasmonic metalenses [31–38]. The patterned metallic film is copper and is assumed as a perfect electric conductor in the simulations. Its detailed structural parameters and cross-sectional views of the SRR metasurface are given in Fig. 2(b). The symmetric complementary SRR is designed to have an open angle of α with respect to the y axis and the same circular groove width of w. The radius and period of the meta-atom are shown by r and p, respectively.

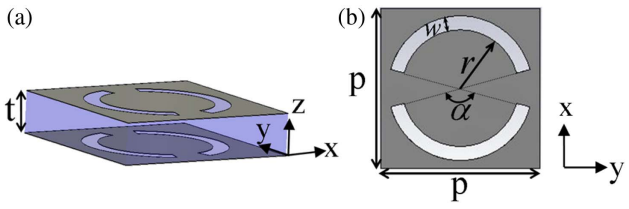

Fig. 2. (a) The perspective views of double-layer identical symmetric split-ring resonator metasurfaces sandwiched by the filled dielectric in between. The thickness is marked by t. (b) The cross-section view and its detailed geometry parameters of the proposed complementary SRR metasurface arranged on the x–y plane.

In order to design an ultra-thin broadband high-efficiency plasmonic metalens based on the above bi-layer SRR phase gradient metasurfaces, its unit cell transmission performances are first simulated and obtained by using commercial CST Microwave Studio based on the finite integrated algorithm. Here, the considered broadband range is within X band, and thus the main structural parameters of the SRR meta-atom are optimized and carefully set as $w = 1$ mm, $p = 11.5$ mm, and $\alpha = 150°$. The phase gradient elements of the metalens are created by varying the radius of r for simplicity. The transmission magnitude and phase changes with different r along the frequency range as indicated by different color lines, are plotted in Figs. 3(a) and 3(b), respectively. It can be noted that an average high transmission magnitude above 80% within the target band from 9 to 12 GHz, as shown by the gray bar, is realized. In addition, the phase slope nearly obeys linear relation both with sufficient change within the considered frequency range for the radius range from 3.5 to 4.7 mm. In the simulations, the unit cell boundary condition along x and y and the open space boundary condition along z are used. The polarization of incident waves is along the x axis in Fig. 2. Compared to the previous double-layer double-SRR broadband metalens [38], the transmission magnitude of the unit cell is much higher, and the meta-atom is also simpler with extended operation bandwidth. Furthermore, the phase change slope of the meta-atom is different; thus, its dispersion of plasmonic metalens is also different. The demonstrated SRR metasurface with proper structural parameters and polarization behaves as a weakly coupled high-contrast resonator, which contributes to its frequency-dependent high transmission. To further verify the high transmission performance of the proposed single SRR meta-atom, the normalized surface current distributions at the central frequency of 11 GHz with different radii of $r = 4.7$ mm, 4.1 mm, and 3.5 mm are plotted in Figs. 4(a), 4(b), and 4(c), respectively. The strong and symmetric corner surface modes around the circular split ring are excited, which contributes to the high transmission performance under the single x-polarized incident wave. Figures 4(d)–4(f) plot the corresponding near-field distributions of the unit cell with different SRR radii. The strong and gradient intensity patterns of near-field distributions further illustrate the linear transmission phase profile of the SRR metasurface with different radii.

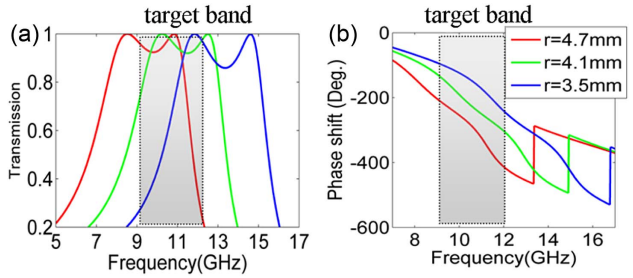

Fig. 3. Transmission performances with different radii of meta-atom for (a) transmission magnitude and (b) phase change distribution along the frequency band, respectively.

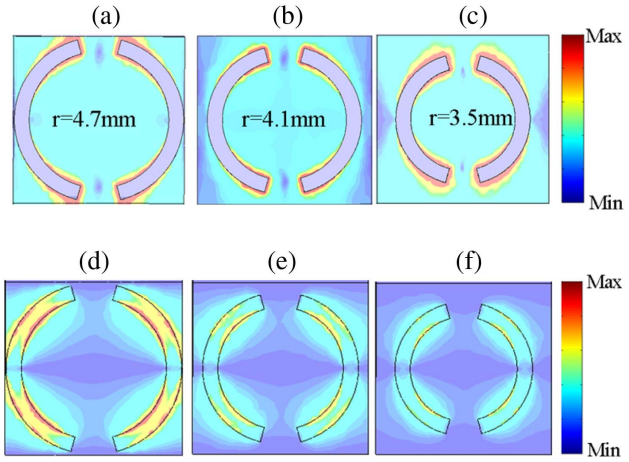

Fig. 4. Normalized surface current distributions of unit cell at 11 GHz with different radii of (a) $r = 4.7$ mm, (b) 4.1 mm, and (c) 3.5 mm, respectively. (d)–(f) The corresponding near-field distributions of the unit cell with different SRR radii.

B. Simulation Results of Broadband Microwave Metalens

Based on the above high-performance transmission of the proposed SRR meta-atoms and the broadband metalens phase profile of Eqs. (1) and (2), a broadband high-efficiency plasmonic metalens is designed by arranging a 15 × 15 square array on the x–y plane with $F = 100$ mm at a central frequency of 11 GHz. The transmission efficiency of the plasmonic metalens is fundamental which is defined by the ratio between the total transmissive plane power to the incident wave power across the whole metalens aperture [39]. Most of the previous plasmonic metalens designs suffer from low transmission efficiency [39–46] especially in the high-frequency band. Here, a very high transmissive efficiency above 80% within the frequency band from 9 to 12 GHz is achieved, as shown by the red dotted line in Fig. 5(a). The relative operation bandwidth is as large as 28.6%. Additionally, an extremely high peak efficiency even above 90% is observed at the central frequency of 11 GHz with an x-polarized incident wave. This is in accord with previous simulated maximum transmission magnitude distributions with different radii of the meta-atom around 11 GHz in Fig. 3(a). Figures 5(b)–5(e) present the normalized power distributions on the transmissive plane just across the metalens aperture for the operation frequency range from 9 to 12 GHz with a 1 GHz step, respectively. The normalized value in each element represents its transmission magnitude of the proposed meta-atom with corresponding varying radii.

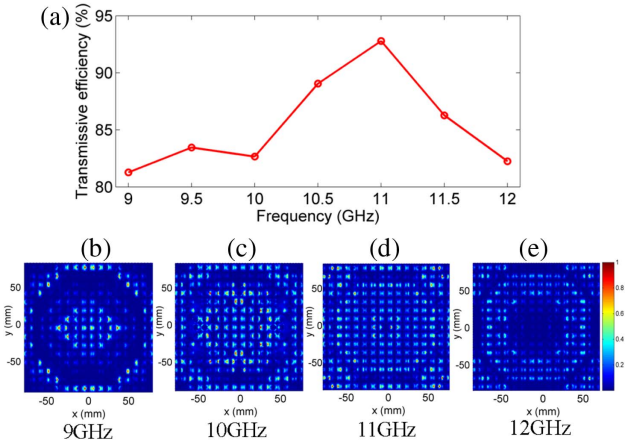

Fig. 5. (a) The simulated transmissive efficiency of the broadband plasmonic metalens ranging from 9 to 12 GHz with a 0.5 GHz step. (b)–(e) are the normalized transmissive plane power patterns for 9 GHz, 10 GHz, 11 GHz, and 12 GHz incident waves, respectively.

The dispersion property of the broadband plasmonic metalens is also highlighted and the focal pattern on the x–z plane for the operation frequency range from 9 to 12 GHz with a 1 GHz step is plotted in Fig. 6(a)–6(d), respectively. The white line indicates its corresponding focal length. Figures 6(e)–6(h) present their corresponding focal spot on the x–y plane. Its detailed simulated focal length distribution along frequency is plotted in Fig. 6(i) as red points with the frequency range from 9 to 12 GHz with a 0.5 GHz step. It is shown that the focal length increases along with operation frequency and thus obeys diffraction-type in Fig. 1(b). This distinct dispersion characteristic is crucial for various applications such as wideband

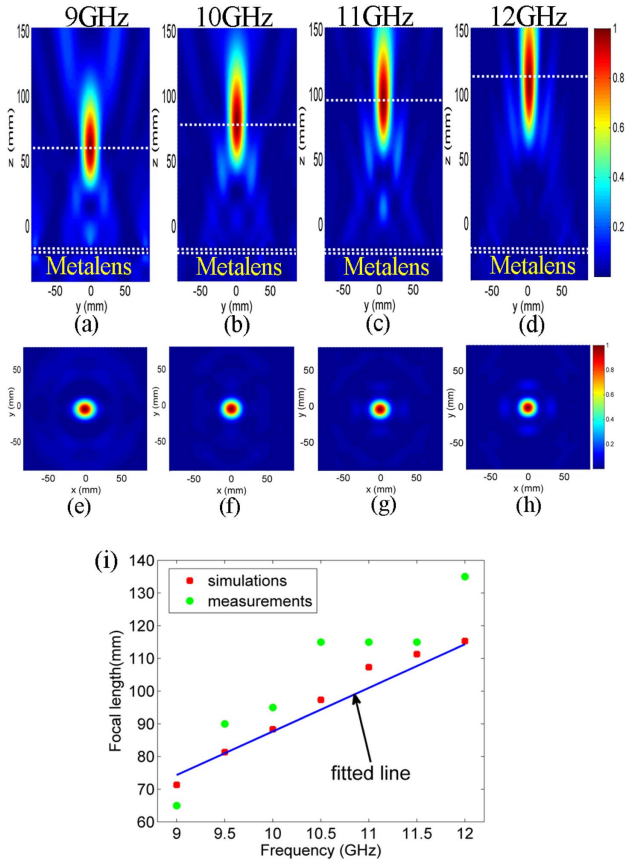

Fig. 6. (a)–(d) The focused power patterns on the x–z plane for 9 GHz, 10 GHz, 11 GHz, and 12 GHz incident waves, respectively. Their corresponding focal lengths are marked by horizontal white line. (e)–(h) are the corresponding focused power patterns on the x–y plane for 9 GHz, 10 GHz, 11 GHz, and 12 GHz incident waves, respectively. (i) The detailed focal length distributions along the frequency range from 9 to 12 GHz both for simulations and measurements. The blue line is the fitting for good viewing for its dispersion property.

microwave transmitarray antenna where antenna location is closely dependent on the varying focal length with different operation frequency [43–56].

C. Sample Fabrications and Experimental Results

Its high-efficiency broadband focusing performances and the diffraction-type dispersion characteristic are also verified by experimental measurements. In the low-frequency microwave regime, plasmonic metalenses are usually fabricated by using the conventional printed circuit board technique. Compared to previous multi-layer broadband metalenses [31–38], a double-layer microwave metalens here only needs a single-step fabrication process and thus is promising for large-scale production. The metallic sheet of the identical double-layer is copper. The filled dielectric is Rogers F4B220 with $\varepsilon = 2.2$ and loss tangent of 0.008. Other parameters are the same as the previous simulations. The detailed experimental setup in the microwave chamber laboratory is illustrated in Fig. 7(a). The source antenna (version is HD-100HA20SZ) emits a broadband linearly-polarized incident wave onto the metalens and a probe on the other side can detect its spatial power distributions at a cross section. The probe is connected to a vector network analyzer (VNA, Agilent N5242A), which can record its focused pattern at a desirable vertical distance across the metalens. The detailed fabricated sample is also given in Fig. 7(b), which is arranged by 15 × 15 square phase gradient transmitarrays.

In order to verify its broadband focusing performance experimentally, the dispersion property of the plasmonic metalens should be set first with the considered broadband frequency range. After some tedious measurements and critical proof, the focal length with frequency range from 9 to 12 GHz with a 0.5 GHz step is obtained and is also plotted in Fig. 6(i) as green points. The fitted blue line of $F = 13 \times (f - 9) + 74$ agrees well with both simulations and measurements; F is the focal length and f is the frequency. Both simulation and measurement results indicate that the focal length increases along with operation frequency and thus obeys diffraction-type dispersion as shown in Fig. 1(b). The measured focal length is slightly larger than simulated results and the maximum error is observed at around 10.5 GHz. This discrepancy may come from the imperfect open-space boundary condition of the measurement environment; the fabrication error of the sample; and the unavoidable misalignment among the source, sample, and probe in the measurement. This negative dispersion is fundamentally different from most of previous broadband metalenses based on plasmonic metasurfaces [34–39] and so provides a new regime to control its dispersion characteristic based on plasmonic metasurfaces. In addition, high-performance focusing along the broadband frequency range of the proposed bilayer plasmonic metalens can extend its potential applications in the microwave regime [43–56].

The measured focused power patterns at the focal length with a frequency range from 9 to 12 GHz with a 1 GHz step are presented in the upper panels in Fig. 8. The focal length at each frequency is based on the measurement results as indicated by green points in Fig. 6(i) correspondingly. Based on the simulated results in Figs. 6(e)–6(h) and the above measured results in Fig. 8, the spot size (full width at half-maximum, FWHM) and its numerical aperture (NA = 0.5λ/FWHM, λ is the working wavelength) can be calculated and compared with each other. The detailed spot size distributions along the x axis are plotted in the lower panels of Fig. 8 for frequencies of 9 GHz, 10 GHz, 11 GHz, and 12 GHz, respectively. The red lines are from simulated results and discrete blue points are from measurement results along its central line. It can be seen that good agreement between simulations and measurements is

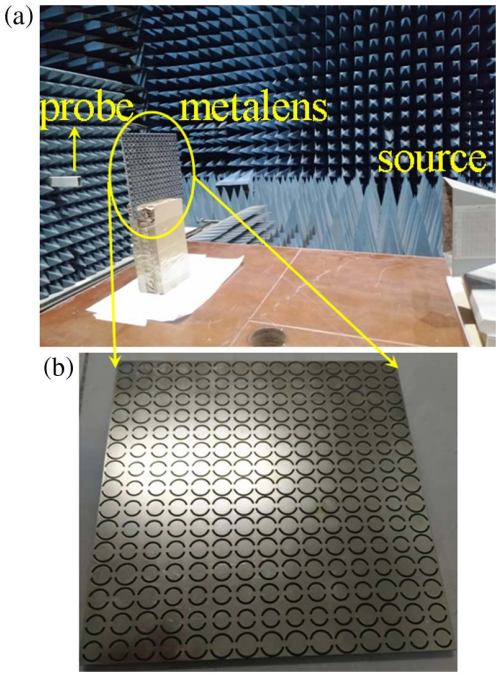

Fig. 7. (a) The diagram of the experimental setup to measure its broadband focusing including source, sample, and probe. (b) The detailed views of the fabricated broadband metalens on the x–y plane.

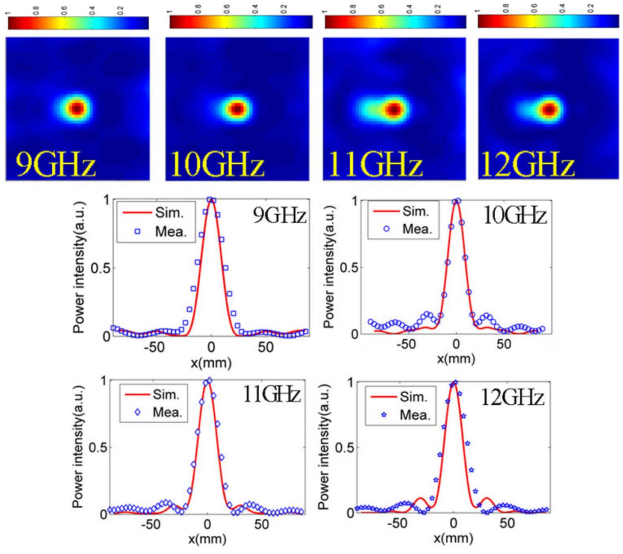

Fig. 8. The measured focused power patterns on the x–y plane and its corresponding focal spot size comparisons between simulations and measurements for 9 GHz, 10 GHz, 11 GHz, and 12 GHz incident waves, respectively.

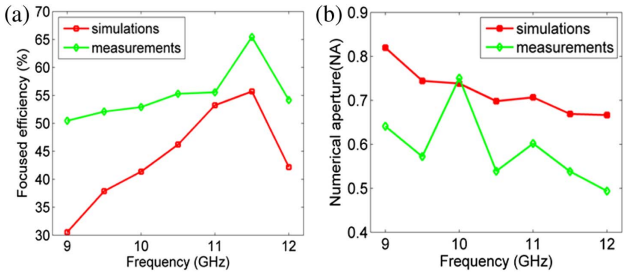

Fig. 9. (a) The measured and simulated focusing efficiency distributions for broadband frequency ranging from 9 to 12 GHz with a 0.5 GHz step. (b) Corresponding spot size and numerical aperture comparisons between simulations and measurements for broadband frequency from 9 to 12 GHz.

realized. To further evaluate its broadband focusing performance, the focusing efficiency is also calculated based on its focal plane with different operation frequencies as shown in Figs. 6(e)–6(h) from 9 to 12 GHz with a 1 GHz step, respectively. The focusing efficiency is defined by the focused power on the focal plane with 3 times FWHM width divided by the incident wave power onto the metalens [36,37,40–42]. The simulated focusing efficiency of the red line in Fig. 9(a) indicates that the high value range 30%–56% with the entire frequency band is obtained with a peak value around 56% at the central frequency of 11.5 GHz. The measured focusing efficiency distribution as a function of operation frequency ranging from 9 to 12 GHz with a 0.5 GHz step is also calculated and plotted as the green line in Fig. 9(a). It is calculated based on the ratio between the focal spot power integration with 3 times FWHM width area in Fig. 8 to the total incident power onto the metalens. It is shown that a much higher focusing efficiency range of 50%–66% is achieved compared to the simulated results in Fig. 5 for a broadband frequency range 9–12 GHz. The maximum value is above 65% at 11.5 GHz, which agrees well with that optimized operation frequency in Fig. 5(a). The presented high working efficiency of the broadband plasmonic metalens can outperform the previous designs in Refs. [31–38]. In addition, the measured large average NA = 0.6 within the entire broadband range is also achieved, as shown by the green points in Fig. 9(b). The measured NA is slightly smaller than the simulated NA = 0.7, as shown by the red lines in the diagram. This can be explained by the larger angular dispersion of the SRR meta-atom at the edge of the metalens. Thus, the refraction angle of θ is decreased in the measurement compared to simulations with ideal boundary conditions [35]. The decreased refraction angle leads to larger focal length and smaller NA according to $\mathrm{NA} = \sin(\arctan\theta)$. Based on the focal length F variation trend in Fig. 6 along the broadband range, the NA also demonstrates a decreased value along with increased frequency which can be explained by $\mathrm{NA} = \sin(\arctan(d/2F))$, where d is the aperture size of the metalens and F increases for diffraction-type dispersion, thus leading to NA decrease along the frequency range. The focusing efficiency is inverse to the NA; thus, the measured results are larger than the simulated ones in Fig. 9(a) [8,9]. This error can be decreased by increasing the focal length of the initial metalens design in simulations. The detailed discussion and analysis are given in Dataset 1, Ref. [64]. The demonstrated broadband high-performance focusing, such as high focusing efficiency, reduced device thickness, and moderate high NA, is very intriguing for various microwave applications such as imaging, sensing, and antennas [43–61]. In addition, the broadband diffraction-type dispersion control can open new regimes in diffractive optics based on plasmonic metasurfaces.

4. CONCLUSIONS

In summary, a broadband plasmonic metalens with only double-layer phase gradient complementary SRR metasurfaces from 9 to 12 GHz (relative bandwidth is 28.6%) is designed and demonstrated both numerically and experimentally. The device thickness is only $0.09\lambda_0$ (λ_0 is the central wavelength). Both numerical simulations and experimental measurements show its increased focal length with increased operation frequency and this negative dispersion characteristic is distinct to traditional refractive-type broadband metalenses. Furthermore, its broadband high-performance focusing such as high working efficiency (both high transmissive efficiency and focusing efficiency) and large NA along the entire broadband frequency range is also achieved in simulations and measurements. These good merits are promising for some high-performance metalens-based applications such as microwave imaging and high-gain antennas, in the low-frequency regime. Also, the demonstrated negative dispersion property can open new avenues to control its dispersion relation based on plasmonic metasurfaces and can facilitate the development of high-quality achromatic plasmonic metalenses in the future.

Funding. National Key Laboratory of Scattering and Radiation.

Acknowledgment. The authors acknowledge helpful discussions with Dr. Liangsheng Li and Dr. Kainan Qi for this work.

Disclosures. The authors declare no conflicts of interest.

Data Availability. The data that support the findings of this study are available from the corresponding author upon reasonable request.

REFERENCES

1. N. Yu, P. Genevet, M. A. Kats, *et al.*, "Light propagation with phase discontinuities: generalized laws of reflection and refraction," Science **334**, 333–337 (2011).
2. Q. He, S. Sun, S. Xiao, *et al.*, "High-efficiency metasurfaces principles, realizations, and applications," Adv. Opt. Mater. **6**, 1800415 (2018).
3. H. Liang, A. Martins, B. Borges, *et al.*, "High performance metalenses: numerical aperture, aberrations, chromaticity, and trade-offs," Optica **6**, 1461–1470 (2019).
4. S. Banerji, M. Meem, A. Majumder, *et al.*, "Imaging with flat optics: metalenses or diffractive lenses?" Optica **6**, 805–810 (2019).
5. J. Engelberg and U. Levy, "The advantages of metalenses over diffractive lenses," Nat. Commun. **11**, 1991 (2020).
6. Y. Zhang, Y. Fu, C. Ma, *et al.*, "Research on fabrication techniques and focusing characteristics of metalens," Coatings **12**, 359 (2022).

7. Z. Wang, Y. Wu, D. Qi, *et al.*, "Progress in design, nanofabrication and performance of metalenses," J. Opt. **24**, 033001 (2022).
8. M. Pan, Y. Fu, M. Zheng, *et al.*, "Dielectric metalens for miniaturized imaging systems progress and challenges," Light Sci. Appl. **11**, 195 (2022).
9. E. Noponen, J. Turunen, and A. Vasara, "Parametric optimization of multilevel diffractive optical elements by electromagnetic theory," Appl. Opt. **31**, 5910–5912 (1992).
10. P. Lalanne, S. Astilean, P. Chavel, *et al.*, "Blazed binary subwavelength gratings with efficiencies larger than those of conventional Échelette gratings," Opt. Lett. **23**, 1081–1083 (1998).
11. U. Levy, E. Marom, and D. Mendlovic, "Thin element approximation for the analysis of blazed gratings simplified model and validity limits," Opt. Commun. **229**, 11–21 (2004).
12. Z. Zhao, M. Pu, H. Gao, *et al.*, "Multispectral optical metasurfaces enabled by achromatic phase transition," Sci. Rep. **5**, 15781 (2015).
13. K. Li, Y. Guo, M. Pu, *et al.*, "Dispersion controlling meta-lens at visible frequency," Opt. Express **25**, 21419–21427 (2017).
14. M. Khorasaninejad, Z. Shi, A. Zhu, *et al.*, "Achromatic metalens over 60 nm bandwidth in the visible and metalens with reverse chromatic dispersion," Nano Lett. **17**, 1819–1824 (2017).
15. E. Arbabi, A. Arbabi, S. Kanali, *et al.*, "Controlling the sign of chromatic dispersion in diffractive optics with dielectric metasurfaces," Optica **4**, 625–632 (2017).
16. W. Zang, Q. Yuan, R. Chen, *et al.*, "Chromatic dispersion manipulation based on metalenses," Adv. Mater. **32**, 1904935 (2019).
17. W. Chen, A. Zhu, J. Sisler, *et al.*, "A broadband achromatic polarization-insensitive metalens consisting of anisotropic nanostructures," Nat. Commun. **10**, 355 (2019).
18. A. Ndao, L. Hsu, J. Ha, *et al.*, "Octave bandwidth photonic fishnet-achromatic metalens," Nat. Commun. **11**, 3205 (2020).
19. R. Jia, Y. Gao, Q. Xu, *et al.*, "Achromatic dielectric metasurface with linear phase gradient in the terahertz domain," Adv. Opt. Mater. **9**, 2001403 (2020).
20. Y. Wang, Q. Chen, W. Yang, *et al.*, "High-efficiency broadband achromatic metalens for near-IR biological imaging window," Nat. Commun. **12**, 5560 (2021).
21. J. Engelberg and U. Levy, "Achromatic flat lens performance limits," Optica **8**, 834–845 (2021).
22. J. Chen, X. Ye, S. Gao, *et al.*, "Planar wide-angle-imaging camera enabled by metalens array," Optica **9**, 431–437 (2022).
23. P. Sun, M. Zhang, F. Dong, *et al.*, "Broadband achromatic polarization insensitive metalens over 950 nm bandwidth in the visible and near-infrared," Chin. Opt. Lett. **20**, 013601 (2021).
24. K. Guo, C. Wang, Q. Kang, *et al.*, "Broadband achromatic metalens with polarization insensitivity in the mid-infrared range," Opt. Mater. **131**, 112489 (2022).
25. H. Lu, B. Zheng, T. Cai, *et al.*, "Frequency-controlled focusing using achromatic metasurface," Adv. Opt. Mater. **9**, 2001311 (2020).
26. F. Presutti and F. Monticone, "Focusing on bandwidth: achromatic metalens limits," Optica **7**, 624–631 (2020).
27. N. Song, N. Xu, J. Gao, *et al.*, "Broadband achromatic and polarization insensitive focused optical vortex generator based on metasurface consisting of anisotropic nanostructures," Front. Phys. **10**, 846718 (2022).
28. K. Ou, F. Yu, G. Li, *et al.*, "Broadband achromatic metalens in mid-wavelength infrared," Laser Photonics Rev. **15**, 2100020 (2021).
29. F. Zhao, Z. Li, S. Li, *et al.*, "Terahertz metalens of hyper-dispersion," Photonics Res. **10**, 886–895 (2022).
30. C. Qin, W. Fan, Q. Wu, *et al.*, "Polarization insensitive achromatic terahertz metalens based on all dielectric metasurfaces," Opt. Commun. **512**, 128061 (2022).
31. C. Williams, Y. Montelongo, and T. D. Wilkinson, "Plasmonic metalens for narrowband dual-focus imaging," Adv. Opt. Mater. **5**, 1700811 (2017).
32. W. Wang, C. Guo, Z. Zhao, *et al.*, "Polarization multiplexing and bifocal optical vortex metalens," Results Phys. **17**, 103033 (2020).
33. M. Hashemi, A. Moazami, M. Naserpour, *et al.*, "A broadband multifocal metalens in the terahertz frequency range," Opt. Commun. **370**, 306–310 (2016).
34. H. Chu, J. Qi, S. Xiao, *et al.*, "A thin wideband high-spatial-resolution focusing metasurface for near-field passive millimeter-wave imaging," Appl. Phys. Lett. **112**, 174101 (2018).
35. C. Qi, X. He, B. Ren, *et al.*, "Broadband terahertz metalenses based on printed circuit board fabrication," Adv. Opt. Mater. **12**, 2302459 (2024).
36. A. A. Fathnan, M. Liu, and D. A. Powell, "Achromatic Huygens' metalenses with deeply subwavelength thickness," Adv. Opt. Mater. **8**, 2000754 (2020).
37. W. Ji, T. Cai, Z. Xi, *et al.*, "Highly efficient and broadband achromatic transmission metasurface to refract and focus in microwave region," Laser Photonics Rev. **16**, 2100333 (2021).
38. Y.-Q. Liu, Z. Ren, Y. Shu, *et al.*, "Broadband, large-numerical-aperture and high-efficiency microwave metalens by using a double-layer transmissive metasurface," Appl. Phys. Express **15**, 014003 (2022).
39. X. He, C. Qi, S. Lei, *et al.*, "Polarization-independent achromatic Huygens' metalens with large numerical aperture and broad bandwidth," Nanophotonics **12**, 3633–3644 (2023).
40. J. Zhang, M. Elkabbash, R. Wei, *et al.*, "Plasmonic metasurfaces with 42.3% transmission efficiency in the visible," Light Sci. Appl. **8**, 53 (2019).
41. Y.-Q. Liu, J. Sun, Y. Che, *et al.*, "High numerical aperture microwave metalens," Opt. Lett. **45**, 6262–6265 (2020).
42. Y.-Q. Liu, J. Sun, Y. Shu, *et al.*, "High numerical aperture and large focusing efficiency metalens based on multilayer transmitarray elements," Opt. Lasers Eng. **147**, 106734 (2021).
43. M. Al-Joumayly and N. Behdad, "Wideband planar microwave lenses using sub-wavelength spatial phase shifters," IEEE Trans. Antennas Propag. **59**, 4542–4552 (2011).
44. A. Boubakri, F. Choubeni, T. Vuong, *et al.*, "A near zero refractive index metalens to focus electromagnetic waves with phase compensation metasurface," Opt. Mater. **69**, 432–436 (2017).
45. J. Qi, Y. Mu, S. Wang, *et al.*, "Birefringent transmissive metalens with an ultradeep depth of focus and high resolution," Photonics Res. **9**, 308–316 (2021).
46. K. Lee, H. Hong, W. Lee, *et al.*, "Broadband metasurface superstrate for polarization-independent wave focusing and gain enhancement at Ka-band," Sci. Rep. **12**, 12015 (2022).
47. S. Tuloti, P. Rezaei, and F. Hamedani, "High-efficient wideband transmitarray antenna," IEEE Antennas Wireless Propag. Lett. **17**, 817–820 (2018).
48. X. Yang, Y. Zhou, L. Xing, *et al.*, "A wideband and low-profile transmitarray antenna using different types of unit-cells," Microw. Opt. Technol. Lett. **61**, 1584–1589 (2019).
49. J. Yang, C. Huang, J. Song, *et al.*, "Metasurface-based lens for antenna gain enhancement and radar cross section reduction," IEEE Photonics J. **11**, 4601809 (2019).
50. X. Y. Li, S. B. Wei, G. Y. Cao, *et al.*, "Graphene metalens for particle nanotracking," Photonics Res. **8**, 1316–1322 (2020).
51. J. Wu, Y. Pan, W. Che, *et al.*, "Design of high-transmittance all-dielectric focusing metasurface with polarization-controllable focus," IEEE Trans. Antennas Propag. **68**, 6183–6192 (2020).
52. I. Derafshi and N. Komjani, "A new high aperture efficiency transmitarray antenna based on Huygens metasurfaces," IEEE Trans. Antennas Propag. **70**, 5458–5467 (2022).
53. Q. Lou and Z. Chen, "Flat-focal-plane dual-metasurface lens for low scan loss and sidelobe level of a metalens antenna," IEEE Trans. Antennas Propag. **70**, 9849–9854 (2022).
54. F. Wu, J. Wang, K. Luk, *et al.*, "A wideband low-profile efficiency-improved transmitarray antenna with over-1-bit phase-shifting elements," IEEE Access **8**, 32163–32169 (2020).
55. D. Serup, G. Pedersen, and S. Zhang, "Combined single-layer K-band transmitarray and beamforming S-band antenna array for sitcom," IEEE Open J. Antennas Propag. **3**, 1134–1140 (2022).
56. S. Pan, W. Shen, Y. Feng, *et al.*, "Miniaturization and performance enhancement of Vivaldi antenna based on ultra-wideband metasurface lens," Int. J. Electron. Commun. **134**, 153703 (2021).
57. Z. Shen, Z. Wang, H. Liu, *et al.*, "Optical trapping and separation of metal nanoparticles by cylindrical metalenses with phase gradients," IEEE Photonics J. **12**, 4600810 (2020).
58. Y. Wang, M. Peng, W. Cheng, *et al.*, "Manipulation force analysis of nanoparticles with ultra-high numerical aperture metalens," Opt. Express **30**, 28479–28491 (2022).

59. J. Zhou, J. Zhao, Q. Wu, *et al.*, "Nonlinear computational edge detection metalens," Adv. Funct. Mater. **32**, 2204734 (2022).
60. A. Karnileli, D. Roitman, M. Liebtrau, *et al.*, "Cylindrical metalens for generation and focusing of free-electron radiation," Nano Lett. **22**, 5641–5650 (2022).
61. Y.-Q. Liu, J. Guo, S. Li, *et al.*, "Low-profile and compact retroreflector enabled by a wide-angle and high-efficiency metalens," Opt. Mater. **134**, 113105 (2022).
62. J. Jung, H. Park, J. Park, *et al.*, "Broadband metamaterials and metasurfaces: a review from the perspectives of materials and devices," Nanophotonics **9**, 3165–3196 (2020).
63. A. Pesarakloo and M. Khalaj-amirhosseini, "Planar, wide-band omnidirectional retroreflector using metal-only transmitarray structure for TE and TM polarizations," Sci. Rep. **12**, 11279 (2022).
64. https://doi.org/10.6084/m9.figshare.25144673.